An Eulerian-Lagrangian localized adjoint method for the advection-diffusion equation

Michael A. Celia

Water Resources Program, Dept. of Civil Engineering and Operations Research, Princeton University, Princeton, NJ 08544, U.S.A.

Thomas F. Russell

Department of Mathematics, University of Colorado at Denver, Denver, CO 80204-5300, U.S.A.

Ismael Herrera

Instituto de Geofísica, UNAM, Apdo. Postal 22-582, 14000 Mexico D.F., Mexico

Richard E. Ewing

Deparment of Mathematics, University of Wyoming, Laramie, WY 82071, U.S.A.

Many numerical methods use characteristic analysis to accommodate the advective component of transport. Such characteristic methods include Eulerian-Lagrangian methods (ELM), modified method of characteristics (MMOC), and operator splitting methods. A generalization of characteristic methods can be developed using an approach that we refer to as an Eulerian-Lagrangian localized adjoint method (ELLAM). This approach is a space-time extension of the optimal test function (OTF) method. The method provides a consistent formulation by defining test functions as specific solutions of the localized homogeneous adjoint equation. All relevant boundary terms arise naturally in the ELLAM formulation, and a systematic and complete treatment of boundary condition implementation results. This turns out to have significant implications for the calculation of boundary fluxes. An analysis of global mass conservation leads to the final ELLAM approximation, which is shown to possess the conservative property. Numerical calculations demonstrate the behaviour of the method with emphasis on treatment of boundary conditions. Discussion of the method includes ideas on extensions to higher spatial dimensions, reactive transport, and variable coefficient equations.

1. INTRODUCTION

Advection-diffusion transport equations are important in many branches of engineering and applied science. These equations are characterized by a nondissipative (hyperbolic) advective transport component and a dissipative (parabolic) diffusive component. When diffusion is the dominant process, virtually all numerical solution procedures perform well. However, when advection is the dominant transport process, most numerical procedures exhibit some combination of excessive nonphysical oscillations and excessive numerical diffusion. While this behaviour is easily explained using, for example, general Fourier analysis[41], the development of numerical schemes that overcome the problems is an ongoing challenge. While extremely fine mesh refinement is one possible solution, it is usually not a feasible alternative due to excessive computational requirements. Thus, alternative numerical formulations are sought that will allow accurate solutions with reasonable computational effort.

Two general classes of approximations can be identified from the literature on modeling advection-dominated transport. The first is referred to herein as the class of optimal spatial methods, while the second is referred to as the class of characteristic methods. Optimal spatial methods (OSM's) employ an Eulerian approach that is rooted in a minimization of error in the approximation of the spatial derivatives. For example, in the pioneering work of Allen and Southwell[1], a finite difference approximation was developed for the advection and diffusion terms that gives exact nodal values for the simplified case of one-dimensional, steady state, constant coefficient advective-diffusive transport without sources, sinks, or reaction terms. This philosophy has persisted in many other aproximations, including the finite element methods of Christie, *et al.*[14], Hughes and coworkers[32-35,46], Carey[9], Barrett and Morton[2], Demkowitcz and Oden[18], Hemker[24], and Celia *et al.*[11-13]. All of the procedures yield an upstream bias in the resulting approximation. While the theoretical basis for many of these methods is

Paper accepted April 1990. Discussion closes June 1991.

impressive, the approximations tend to be ineffective in transient simulations because of the strong influence of the time derivative. The salient features of this class of approximations may be summarized as follows: (*i*) time truncation error dominates the solutions (*ii*) solutions are characterized by significant numerical diffusion and some phase errors (*iii*) the Courant number ($Cu \equiv V\Delta t/\Delta x$) is generally restricted to be less than one, and sometimes much less than one. A general comparison of some of these methods is provided by Bouloutas and Celia[5].

Other Eulerian methods can be developed that perform significantly better than OSM approximations. These methods attempt to use a nonzero spatial truncation error (thereby differing from OSM's) to cancel temporal errors and thereby reduce the overall truncation error. The cubic Petrov-Galerkin method of Bouloutas and Celia[6] and the general $N + 2$ methods of Westerink and coworkers[8,48] are examples of such procedures. While improved accuracy results from these formulations, they still suffer from strict Courant number limitations.

Because of the hyperbolic nature of advective transport, it is natural to look to characteristic analysis to aid in solving the problem. This philosophy has led to many related approximation techniques, which are called by a variety of names, including Eulerian-Lagrangian methods (ELM)[3,37-39], transport diffusion method[4,31,42], method of characteristics (MOC)[40], modified method of characteristics (MMOC)[19,23,44], and operator splitting methods[15,21,49]. These will be grouped herein under the title of characteristic methods (CM's). Each of these methods has in common the fact that the advective component is treated by a characteristic tracking algorithm (a Lagrangian frame of reference), and the diffusive step is treated separately using a more standard (Eulerian) spatial approximation. These methods have the significant advantage that Courant number restrictions of purely Eulerian methods are alleviated because of the Lagrangian nature of the advection step. Furthermore, because the spatial and temporal dimensions are coupled through the characteristic tracking, the influence of time truncation error present in OSM approximations is greatly reduced.

This paper and a companion one[30] provide a generalization of characteristic methods using an approach that we refer to as a localized adjoint method (LAM). The present paper begins by reviewing the LAM procedure, including discussion of the general approach as well as specific formulations that have been developed to date. This is followed by the specific space-time LAM formulation that naturally leads to a generalized CM approximation. This approach provides a consistent formulation that does not rely on any operator splitting or equation decomposition. In addition, all relevant boundary terms arise naturally in the formulation, and a systematic and complete treatment of boundary condition implementation is presented. This turns out to have significant implications for the calculation of boundary fluxes. An analysis of global mass conservation then leads to the final ELLAM approximation, which is shown to possess the conservative property. Example calculations are presented to illustrate the method. Finally, a discussion of several additional topics is presented, including extension to multiple dimensions, development of higher order methods, formulations for reactive transport equations, and treatment of nonconstant coefficients. The companion paper dwells more thoroughly on the associated theoretical questions.

2. LOCALIZED ADJOINT METHODS

The general approach of localized adjoint methods (LAMs) is based on the philosophy of the algebraic theory of numerical methods presented by Herrera[10,25-29]. In LAM, a weight or test function, call it $w_k(\mathbf{w})$, is used to write a weak form of the governing differential equation of interest. Let the governing differential operator be denoted symbolically by $\mathcal{L}$, with the governing equation written as

$$\mathcal{L}u(\mathbf{x}) = f(\mathbf{x}), \quad \mathbf{x} \in \Omega, \tag{1}$$

where u is the dependent variable and $\mathbf{x}$ is the vector of independent variables. The weak form of equation (1) is written as

$$\int_\Omega (\mathcal{L}u)w_k(\mathbf{x})d\mathbf{x} = \int_\Omega f(\mathbf{x})w_k(\mathbf{x})d\mathbf{x}. \tag{2}$$

In the general LAM approach, the domain Ω is discretized into a number of subintervals or elements $\Omega_e (e = 1, 2, \ldots, E)$. Equation (2) is then written as a sum of elemental boundary integrals and integrals over the interior of each element. Depending on the continuity of u and w_k, this may be done using simple integration-by-parts, using the theory of distributions, or using the general Green's formulas of Ref. 26. This point is discussed in detail in the companion paper[30]. The resulting interior integrals involve an integrand that includes the adjoint of $\mathcal{L}$ acting on w_k, $\mathcal{L}^*w_k$. The LAM procedure then defines as test functions those which satisfy the homogeneous adjoint equation within each element, so that $\mathcal{L}^*w_k = 0$. Therefore all interior elemental integrals are eliminated and only boundary integrals remain to be evaluated. Evaluation of these boundary terms leads to the algebraic approximation of interest. The key to LAM algorithms is the choice of subintervals $\{\Omega_e\}$ and the definition of test functions that locally satisfy the homogeneous adjoint operator. This latter point implies that the test functions vary as the operator varies. In this way, the test functions reflect the physics inherent in the governing equation.

LAM approximations have been applied to ordinary differential equations[10,28,29] and to the spatial dimensions of partial differential equations[11-13]. For ordinary differential equations, optimal approximations can be obtained in the sense that exact nodal values are achieved for the case of constant coefficients and approximations of an arbitrarily high order can be achieved for the case of variable coefficients. These results apply for arbitrary forcing functions and arbitrary boundary conditions. Partial differential equations in multiple spatial dimensions have been solved by forming tensor product test functions[11]. For transient partial differential equations, the LAM approach has been applied in space to achieve a semi-discretization for the linear advection-diffusion equation[12] as well as nonlinear advection-diffusion-reaction systems of transport equations[13]. Standard time-marching algorithms were then used to solve the semi-discrete system. When applied to the advection-diffusion equation, the semi-discrete LAM forms an optimal spatial method. This method therefore suffers from the limitations of all optimal spatial methods, as described in the previous section. However, there is no reason for the LAM approach to be restricted to semi-discrete formulations. Because the LAM approach is quite general, LAM approximations can be applied to the full

space-time operator. The next section develops a space-time LAM algorithm that produces a general characteristic method algorithm.

3. AN EULERIAN-LAGRANGIAN LAM FOR ADVECTION-DIFFUSION TRANSPORT EQUATIONS

Consider the one-dimensional transient advection-diffusion equation subject to appropriate initial and boundary conditions,

$$\mathcal{L}u \equiv \frac{\partial u}{\partial t} + V\frac{\partial u}{\partial x} - D\frac{\partial^2 u}{\partial x^2} = f(x, t),$$
$$x \in \Omega_x = [0, l]$$
$$t \in \Omega_t = [0, \infty]$$
$$(x, t) \in \Omega_{x,t} \equiv \Omega_x \times \Omega_t, \tag{3}$$
$$u(x, 0) = u_I(x)$$
$$u(0, t) = u_0(t)$$
$$\frac{\partial u}{\partial x}(l, t) = q_l(t).$$

First- and second-type boundary conditions are chosen for demonstration purposes only; the following development accommodates any combination of boundary conditions. The adjoint operator associated with the operator $\mathcal{L}$ of equation (3) is

$$\mathcal{L}^* w = \frac{\partial w}{\partial t} - V\frac{\partial w}{\partial x} - D\frac{\partial^2 w}{\partial x^2}. \tag{4}$$

The LAM approach is initiated by writing the weak form of equation (3). Let $w(x, t)$ refer to a test function (whose precise form will be determined as part of the LAM development), so that the weak form of equation (3) is

$$\int_0^\infty \int_0^l (\mathcal{L}u - f)w(x, t)\,dx\,dt = 0. \tag{5}$$

As discussed in the previous section, the test function $w(x, t)$ is chosen from the solution space of the homogeneous adjoint equation. In this case, the homogeneous adjoint equation is

$$\mathcal{L}^* w = -\frac{\partial w}{\partial t} - V\frac{\partial w}{\partial x} - D\frac{\partial^2 w}{\partial x^2} = 0. \tag{6}$$

As opposed to the simple developments for ordinary differential operators, the solution space of the partial differential equation (6) is infinite-dimensional. Because the objective of the numerical procedure is derivation of a finite number of algebraic equations, only a finite number of test functions should be chosen. Different choices of test functions (solutions of equation (6)) lead to different classes of approximations, including families of optimal spatial methods and general characteristics methods.

By analogy to the tensor product approach of Celia *et al.*[11], a product solution of the form $w(x, t) = \xi(x)\tau(t)$ could be sought such that $\xi(x)$ satisfies the homogeneous spatial operator of equation (6) while $\tau(t)$ satisfies the temporal part. Such a space-time split, defined on a rectangular discretization of $\Omega_{x,t}$, leads to optimal spatial algorithms involving exponential weightings in space. The result is analogous to the semi-discretizations presented by Celia *et al.*[12,13].

To derive a general family of characteristic methods (CM's), a different set of solutions to equation (6) must be used. In particular, consider solutions to equation (6) which satisfy the two homogeneous sub-equations that are grouped based on common order of derivatives, viz. $(\partial w/\partial t) + V(\partial w/\partial x) = 0$ and $D(\partial^2 w/\partial x^2) = 0$. The second constraint implies linear functions of x, while the first constraint implies w = constant along lines $x - x_0 = V(t - t_0)$. A natural choice for such a test function can be defined with respect to a rectangular array of nodes in space-time as follows,

$$w_i^{n+1}(x, t) = \begin{cases} \dfrac{x - x_{i-1}}{\Delta x} + V\dfrac{t^{n+1} - t}{\Delta x}, & (x, t) \in \Omega_1^i, \\ \dfrac{x_{i+1} - x}{\Delta x} - V\dfrac{t^{n+1} - t}{\Delta x}, & (x, t) \in \Omega_2^i, \\ 0, & \text{all other } (x, t), \end{cases} \tag{7}$$

where subscript i denotes spatial location ($x_i \equiv i(\Delta x)$ for constant spatial step Δx), superscript n denotes time level ($t^n \equiv n(\Delta t)$ for constant time step Δt), and the test function $w_i^{n+1}(x, t)$ is associated with spatial location i and temporal location $n + 1$. In writing equation (7), constant node spacing Δx has been assumed. The regions Ω_1^i and Ω_2^i are illustrated in Fig. 1, as is a typical test function. The function $w_i^{n+1}(x, t)$ has the properties that it is

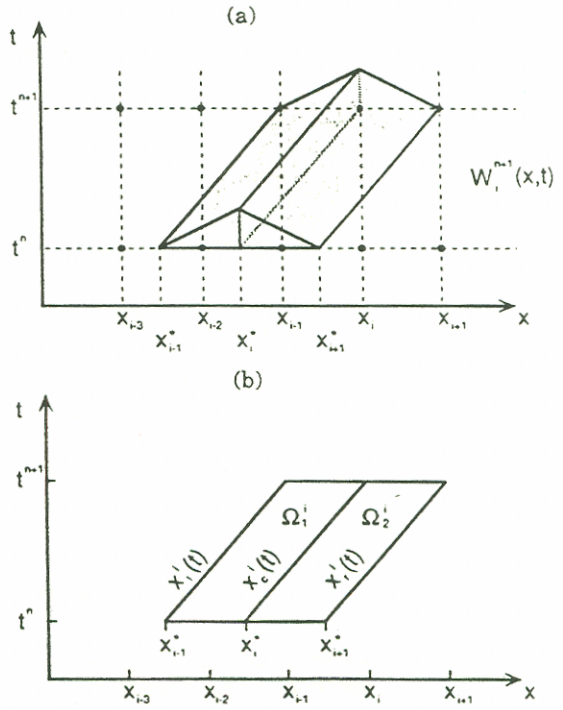

Fig. 1. (a) General interior test function $w_i^{n+1}(x, t)$, and (b) associated geometric definitions

$\mathbb{C}^0[\Omega_x]$, $\mathbb{C}^{-1}[\Omega_t]$, is nonzero over only one time step (t^n to t^{n+1}) with discontinuities aligned along t^n and t^{n+1}, and the lines of spatial derivative discontinuities align with the characteristics that intersect the nodes x_{i-1}, x_i, and x_{i+1} at time level t^{n+1}.

Given this test function definition, the weak form of the equation can be evaluated by standard integration procedures. Let the spatial locations at time level t^n that are on the characteristic curves that intersect points x_{i-1}, x_i, x_{i+1} at t^{n+1} be denoted as x^*_{i-1}, x^*_i, and x^*_{i+1}, respectively, as illustrated in Fig. 1. These points are often referred to as the 'foot of the characteristic' points. In addition, let the characteristic curves that pass through points x_{i-1}, x_i, and x_{i+1} at time t^{n+1} be identified by $x^i_l(t)$, $x^i_c(t)$, and $x^i_r(t)$, respectively, as illustrated in Fig. 1. The weak form of equation (3) can be rewritten in an equivalent form by applying integration by parts. If $u(x, t)$ is assumed to be at least $\mathbb{C}^1$-continuous in x and $\mathbb{C}^0$-continuous in t (cases of less restrictive continuity are treated in the companion paper[30]), then the integrations of equation (5) can be written equivalently as a sum of elemental integrals. Integration by parts can then be applied element-by-element, where 'elements' are defined as the regions Ω^i_1, Ω^i_2, etc. Evaluation of the weak form (5), with $w_i^{n+1}(x, t)$ used as the test function, leads to the following expression.

$$
\begin{aligned}
&\int_0^\infty \int_0^l (\mathcal{L}u - f) w_i^{n+1}(x, t)\,dx\,dt = 0 \\
&= \int_0^\infty \int_0^l \left[\frac{\partial u}{\partial t} + V\frac{\partial u}{\partial x} - D\frac{\partial^2 u}{\partial x^2} - f(x, t)\right] w_i^{n+1}(x, t)\,dx\,dt \\
&= \int_{x_{i-1}}^{x_{i+1}} u(x, t^{n+1}) w_i^{n+1}(x, t^{n+1})\,dx \\
&\quad - \int_{x^*_{i-1}}^{x^*_{i+1}} u(x, t^n) w_i^{n+1}(x, t^n)\,dx \\
&\quad - D\left[\int_{t^n}^{t^{n+1}} u(x^i_l(t), t) \left[\!\left[\frac{\partial w_i^{n+1}}{\partial x}\right]\!\right]_{x^i_l(t)} dt\right. \\
&\quad + \int_{t^n}^{t^{n+1}} u(x^i_c(t), t) \left[\!\left[\frac{\partial w_i^{n+1}}{\partial x}\right]\!\right]_{x^i_c(t)} dt \\
&\quad \left. + \int_{t^n}^{t^{n+1}} u(x^i_r(t), t) \left[\!\left[\frac{\partial w_i^{n+1}}{\partial x}\right]\!\right]_{x^i_r(t)} dt\right] \\
&\quad + \int_{\Omega^i_1} u(x, t)\mathcal{L}^* w_i^{n+1}\,dx\,dt \\
&\quad + \int_{\Omega^i_2} u(x, t)\mathcal{L}^* w_i^{n+1}\,dx\,dt \\
&\quad - \int_{\Omega^i_1 \cup \Omega^i_2} f(x, t) w_i^{n+1}(x, t)\,dx\,dt = 0, \qquad (8)
\end{aligned}
$$

where the double bracket notation denotes a spatial jump operator, $[\![\,\cdot\,]\!]_{x_s} \equiv \lim_{\epsilon \to 0}[(\cdot)_{x_s+\epsilon} - (\cdot)_{x_s-\epsilon}]$. Due to the special choice of test function given by equation (7), $\mathcal{L}^* w_i^{n+1} = 0$ in both Ω^i_1 and Ω^i_2, so that the interior integrals involving $u(x, t)$ are eliminated. Furthermore, the spatial jump operators can be evaluated explicitly from equation (7) as

$$
\left[\!\left[\frac{\partial w_i^{n+1}}{\partial x}\right]\!\right]_{x^i_l(t)} = \left[\!\left[\frac{\partial w_i^{n+1}}{\partial x}\right]\!\right]_{x^i_c(t)} = \frac{1}{\Delta x},
$$

$$
\left[\!\left[\frac{\partial w_i^{n+1}}{\partial x}\right]\!\right]_{x^i_r(t)} = \frac{-2}{\Delta x}.
$$

Equation (8) can therefore be simplified as

$$
\begin{aligned}
&\int_{x_{i-1}}^{x_{i+1}} u(x, t^{n+1}) w_i^{n+1}(x, t^{n+1})\,dx \\
&\quad - \int_{x^*_{i-1}}^{x^*_{i+1}} u(x, t^n) w_i^{n+1}(x, t^n)\,dx \\
&\quad - D\left[\left(\frac{1}{\Delta x}\right)\int_{t^n}^{t^{n+1}} u(x^i_l(t), t)\,dt\right. \\
&\quad - \left(\frac{2}{\Delta x}\right)\int_{t^n}^{t^{n+1}} u(x^i_c(t), t)\,dt \\
&\quad \left. + \left(\frac{1}{\Delta x}\right)\int_{t^n}^{t^{n+1}} u(x^i_r(t), t)\,dt\right] \\
&\quad = \int_{\Omega^i_1 \cup \Omega^i_2} f(x, t) w_i^{n+1}(x, t)\,dx\,dt. \qquad (9)
\end{aligned}
$$

Equations (7) through (9) have been written under the assumptions of constant node spacing Δx and constant coefficients in the governing equation, and for characteristics that do not intersect the spatial boundaries. For nonconstant spacing, the test functions change as follows:

$$
w_i^{n+1}(x, t) = \begin{cases} \dfrac{x - x_{i-1}}{\nabla x_i} + V\dfrac{t^{n+1} - t}{\nabla x_i}, & (x, t) \in \Omega^i_1, \\ \dfrac{x_{i+1} - x}{\Delta x_i} - V\dfrac{t^{n+1} - t}{\Delta x_i}, & (x, t) \in \Omega^i_2 \\ 0, & \text{all other } (x, t), \end{cases} \qquad (10)
$$

where $\nabla x_i \equiv x_i - x_{i-1}$ and $\Delta x_i \equiv x_{i+1} - x_i$ are the usual backward and forward difference operators. This modification does not change equation (8), and equation (9) is modified only by a revised determination of the locations x^*_{i-1}, x^*_i, x^*_{i+1}, and by the evaluation of spatial jumps, which are now

$$
\left[\!\left[\frac{\partial w_i^{n+1}}{\partial x}\right]\!\right]_{x^i_l(t)} = \frac{1}{\nabla x_i}, \quad \left[\!\left[\frac{\partial w_i^{n+1}}{\partial x}\right]\!\right]_{x^i_r(t)} = \frac{1}{\Delta x_i},
$$

$$
\left[\!\left[\frac{\partial w_i^{n+1}}{\partial x}\right]\!\right]_{x^i_c(t)} = \left(\frac{1}{\nabla x_i} + \frac{1}{\Delta x_i}\right)
$$

When the velocity coefficient in the governing equation is not constant, the characteristics are, in general, not

parallel. The definition of the test function then must be modified to reflect this fact. This case is discussed in some detail in Section 8 of this paper. One possibility for this case is to assume that the locations of characteristic lines between the characteristics that pass through adjacent nodes at t^{n+1} are determined by linear interpolation in space for all $t^n \le t \le t^{n+1}$. Then the appropriate test function is

$$w_i^{n+1}(x, t) = \begin{cases} \dfrac{x - x_{i-1}}{x_c^i(t) - x_l^i(t)} + V\dfrac{t^{n+1} - t}{x_c^i(t) - x_l^i(t)}, & (x, t) \in \Omega_1^i, \\ \dfrac{x_{i+1} - x}{x_r^i(t) - x_c^i(t)} - V\dfrac{t^{n+1} - t}{x_r^i(t) - x_c^i(t)}, & (x, t) \in \Omega_2^i \\ 0, & \text{all other } (x, t). \end{cases} \tag{11}$$

For this case, the only change in the resulting numerical approximation is again in the location of the feet of the characteristics and in the spatial jumps. Now the jumps are functions of time, viz.,

$$\left[\!\left[\frac{\partial w_i^{n+1}}{\partial x} \right]\!\right]_{x_c^i(t)} = \frac{1}{x_c^i(t) - x_l^i(t)},$$

$$\left[\!\left[\frac{\partial w_i^{n+1}}{\partial x} \right]\!\right]_{x_r^i(t)} = \frac{1}{x_r^i(t) - x_c^i(t)},$$

$$\left[\!\left[\frac{\partial w_i^{n+1}}{\partial x} \right]\!\right]_{x_c^i(t)} = -\left[\frac{1}{x_c^i(t) - x_l^i(t)} + \frac{1}{x_r^i(t) - x_c^i(t)} \right]$$

Because these terms are functions of time, they cannot be removed from the integrations of equation (8). The resulting approximation is thus of the form

$$\begin{aligned} &\int_{x_{i-1}}^{x_{i+1}} u(x, t^{n+1}) w_i^{n+1}(x, t^{n+1})\, dx \\ &- \int_{x_{i-1}^*}^{x_{i+1}^*} u(x, t^n) w_i^{n+1}(x, t^n)\, dx \\ &- D\left[\int_{t^n}^{t^{n+1}} \left[\frac{1}{x_c^i(t) - x_l^i(t)} \right] u(x_l^i(t), t)\, dt \right. \\ &- \int_{t^n}^{t^{n+1}} \left[\frac{1}{x_c^i(t) - x_l^i(t)} + \frac{1}{x_r^i(t) - x_c^i(t)} \right] u(x_c^i(t), t)\, dt \\ &\left. + \int_{t^n}^{t^{n+1}} \left[\frac{1}{x_r^i(t) - x_c^i(t)} \right] u(x_r^i(t), t)\, dt \right] \\ &= \int_{\Omega_1^i \cup \Omega_2^i} f w_i^{n+1}\, dx\, dt. \end{aligned} \tag{12}$$

In the developments that follow, V and Δx are held constant. This allows the general ideas of the method to be demonstrated clearly.

Because of the special test functions chosen, this class of LAM is referred to as an Eulerian-Lagrangian LAM (ELLAM). Notice that the unknown function $u(x, t)$ has not yet been approximated by any specific functional form. The integrals that appear in this equation may in fact be approximated in many different ways. Different approximations of these integrals lead to different CM algorithms reported in the literature. In all of these, the integrals are approximated in terms of nodal values of u at the discrete time levels t^n and t^{n+1}, so that the unknowns in the equation ultimately include the nodal values at time t^{n+1}, $\{U_0^{n+1}, U_1^{n+1}, \ldots, U_E^{n+1}\}$, where U_i^{n+1} is an approximation to $u(x_i, t^{n+1})$. For example, piecewise linear spatial interpolation of u at time levels t^{n+1} and t^n, coupled with a one-point (at $t = t^{n+1}$) fully implicit approximation to the temporal integrals, leads to the modified method of characteristics (MMOC) of Douglas and Russell[19] and others. Given the definition of the test function $w_i^{n+1}(x, t)$, and the assumptions of constant Δx and V, the resulting discrete approximation is

$$\begin{aligned} &\left(\frac{\Delta x}{6}\right) U_{i+1}^{n+1} + \left(\frac{2\Delta x}{3}\right) U_i^{n+1} + \left(\frac{\Delta x}{6}\right) U_{i+1}^{n+1} \\ &-(\Delta x)[\beta_1 U_{i-Nc-2}^n + \beta_2 U_{i-Nc-1}^n \\ &+\beta_3 U_{i-Nc}^n + \beta_4 U_{i-Nc+1}^n] \\ &-\frac{D(\Delta t)}{\Delta x}[U_{i+1}^{n+1} - 2U_i^{n+1} + U_{i-1}^{n+1}] = F_i^{n-1}, \end{aligned} \tag{13}$$

where Nc is the (truncated) integer value of the Courant number Cu

$$\mathrm{Cu} \equiv \frac{V\Delta t}{\Delta x}, \quad \alpha \equiv 1 - [\mathrm{CU} - \mathrm{Nc}],$$

$$\beta_1 = \frac{1}{6} - \frac{\alpha}{2} + \frac{\alpha^2}{2} - \frac{\alpha^3}{6},$$

$$\beta_2 = \frac{2}{3} - \alpha^2 + \frac{\alpha^3}{2},$$

$$\beta_3 = \frac{1}{6} + \frac{\alpha}{2} + \frac{\alpha^2}{2} - \frac{\alpha^3}{2},$$

and

$$\beta_4 = \frac{\alpha^3}{6}.$$

The grouping of terms involving β_i corresponds to exact evaluation of the integral at $t = t^n$, namely

$$\int_{x_{i-1}^*}^{x_{i+1}^*} u(x, t^n) w_i^{n+1}(x, t^n)\, dx,$$

using piecewise linear interpolation for $u(x, t^n)$ and assuming constant Δx. The usual MMOC approach approximates this term using numerical integration, which is the most practical option for nonconstant grid spacing and/or nonconstant velocity fields. The exact integration is used here for demonstration purposes only, and to indicate that it is a reasonable option when both Δx and V are constant. Baptista[3] has compared a variety of interpolation schemes for the integrals at time t^n in the context of Eulerian-Lagrangian Methods. These procedures are

closely related to MMOC and are again a subset of the general CM equations that result from ELLAM.

Traditional MMOC and ELM algorithms have a substantial base of theoretical results[17,19,23,44] and computational experience[3,37–39,45]. However, several problems remain unresolved. Chief among them are treatment of boundary conditions and evaluation of spatial integrals along $t = t^n$. Significant experience has been gained in integral evaluation (see, for example, Ref. 3). However, as discussed by Russell[43], boundary conditions have usually been dealt with in *ad hoc* ways. When a characteristic line passing through points x_{i-1}, x_i, or x_{i+1} at time t^{n+1} crosses the boundary between times t^n and t^{n+1}, call it time t^*, the boundary information must be incorporated into the approximating equation. Dirichlet conditions are easiest to deal with, although most algorithms fail to accommodate the reduced time interval $t^{n+1} - t^*$ associated with certain boundary terms (see Section 4). Flux boundary conditions are usually ignored, although some developments appear in the literature (e.g., Ref. 38). Based on the treatment of boundary conditions, all MMOC and ELM approximations proposed in the literature appear to be inherently non-mass-conservative. In variable-velocity flow fields, failure to conserve mass also results from inexact representations of the characteristics.

The ELLAM approach outlined above overcomes the boundary condition and mass conservation problems inherent in other CM approaches. As the next section demonstrates, the ELLAM approach provides a systematic and consistent methodology for proper incorporation of boundary conditions. Correct treatment of boundary conditions leads to an overall approximation that can be shown to possess the conservative property, thereby assuring conservation of mass in the numerical solution. Therefore, while ELLAM provides a general framework from which many traditional ELM and MMOC approximations can be derived, it also provides important additions to the methods by properly incorporating boundary information and by possessing demonstrable mass conservation. In Section 8, conservation in the case of approximate characteristics dictated by variable velocity fields will be discussed.

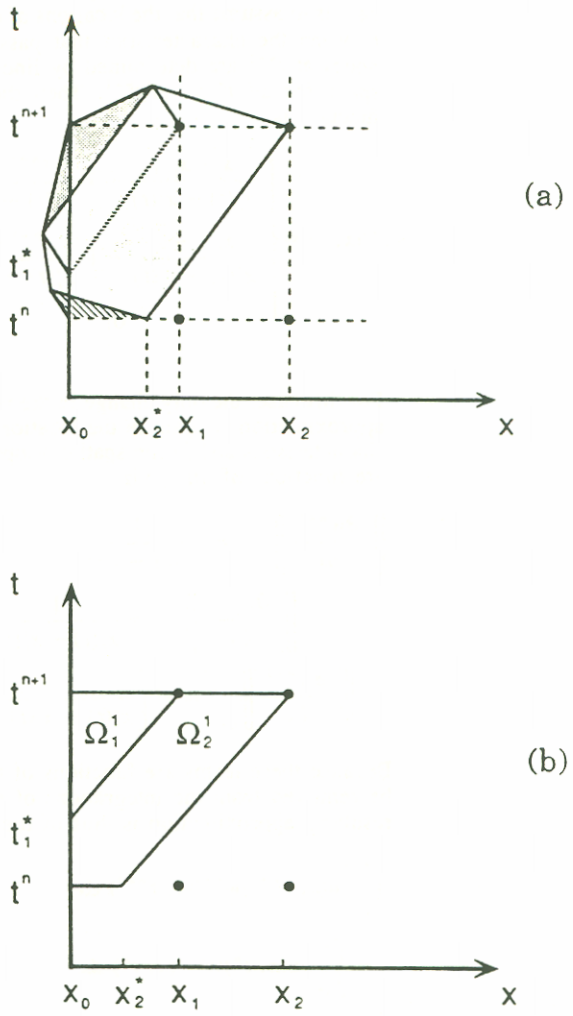

Fig. 2. (a) Test function $w_i^{n+1}(x, t)$, and (b) associated geometric definitions

4. IMPLEMENTATION OF BOUNDARY CONDITIONS

The general CM equation (12) must be modified when one or more of the characteristic curves $x_i^i(t)$, $x_c^i(t)$, $x_f^i(t)$ intersects the spatial boundary. When this occurs, boundary conditions are introduced into the approximating equations. Proper evaluation of the weak form, (8) inherently accommodates all relevant boundary information, and provides for proper incorporation of boundary conditions at all boundaries. As the following derivation demonstrates, careful treatment of both inflow and outflow boundaries allows proper incorporation of boundary conditions and provides a formulation that demonstrably conserves global mass. In addition, the ELLAM equations apply to both the advection-diffusion ($D \neq 0$) and pure advection ($D = 0$) cases with no modification of the equations required as $D \to 0$.

To demonstrate the incorporation of boundary conditions at the inflow boundary ($x = x_0 = 0$ for the example of equation (3) with $V > 0$), let us consider an example for which the Courant number $\mathrm{Cu} \equiv [V(\Delta t)/(\Delta x)]$ is between 1 and 2. The general case of arbitrary Cu is treated in the appendix. For the case of $1 \leq \mathrm{Cu} < 2$, the characteristic curve that passes through node 1 ($x = x_1$) at time t^{n+1} intersects the boundary at $x = x_0 = 0$ at time $t_1^* \geq t^n$. Therefore, equations that involve this characteristic will be influenced by boundary conditions. Consider the ELLAM equation associated with node 1. The test function $w_1^{n+1}(x, t)$, illustrated in Fig. 2, differs from the general function w_i^{n+1} of Fig. 1 because part of w_1^{n+1} intersects the boundary at $x = 0$ with nonzero value. Therefore, evaluation of the general ELLAM equation (7) is modified by boundary influences. The ELLAM equation associated with $w_1^{n+1}(x, t)$ is derived in the same way as equations (8) and (9): elemental integration by parts is applied to each term, the condition that $\mathcal{L}^* w_1^{n+1} = 0$ in each element is recognized, and the appropriate jumps in the spatial derivative $[\![(\partial w/\partial x)]\!]$ are evaluated to

produce

$$\int_{x_0}^{x_2} u(x, t^{n-1}) w_1^{n+1}(x, t^{n+1})\, dx - \left[\int_{x_0}^{x_1^*} u(x, t^n) w_1^{n+1}(x, t^n)\, dx + V \int_{t^n}^{t^{n-1}} u(0, t) w_1^{n+1}(0, t)\, dt \right] - D\left[\left(\frac{1}{\Delta x}\right) \int_{t_1^*}^{t^{n-1}} u(0, t)\, dt - \left(\frac{2}{\Delta x}\right) \int_{t_1^*}^{t^{n-1}} u(x_c^1(t), t)\, dt + \left(\frac{1}{\Delta x}\right) \int_{t^n}^{t^{n-1}} u(x_r^1(t), t)\, dt \right] + D \int_{t^n}^{t^{n-1}} \frac{\partial u}{\partial x}(0, t) w_1^{n+1}(0, t)\, dt + D\left(\frac{1}{\Delta x}\right) \int_{t^n}^{t_1^*} u(0, t)\, dt = \int_{\Omega_1^1 \cup \Omega_2^1} f(x, t) w_1^{n+1}(x, t)\, dx\, dt. \quad (14)$$

Examination of equation (14) indicates that the spatial integration at time t^n is modified by the boundary at $x = 0$. While this integration spans a distance of $2\Delta x$ in equation (7), it spans $(2 - \mathrm{Cu})\Delta x$ in equation (14). The part that is cut off by the boundary, corresponding to the distance $\mathrm{Cu}(\Delta x)$, is picked up by the third integral on the left side of equation (14), which involves the boundary value $u(0, t)$. The next three integrals in equation (14) correspond to the three diffusive terms in equation (7), except that the left integral is evaluated along $x = 0$ and the integrand is the boundary value $u(0, t)$. Finally, the last two integrals on the left side of equation (14) are again integrals that are evaluated along the boundary $x = 0$: the second of these involves the function $u(0, t)$ but the first involves the spatial gradient $(\partial u/\partial x)(0, t)$. Notice that this latter integral introduces an additional degree of freedom at the boundary, so that both $u(0, t)$ and $(\partial u/\partial x)(0, t)$ are present in this equation. Even when a first type boundary condition is specified at $x = 0$, the flux at the boundary may need to be determined due to the presence of this integral. Therefore, an additional equation should be written, that which corresponds to node 0, with test function $w_0^{n+1}(x, t)$ (see Fig. 3). This is in contrast to standard finite element methods, wherein the boundary flux need not be explicitly determined when first type boundary conditions are prescribed. The reason that both boundary values appear in the ELLAM formulation is that the space-time LAM elements of Fig. 1 are not parallel to the time axis, while standard semidiscrete finite elements correspond to rectangular space-time elements with sides parallel to the space-time coordinate axes.

Similar terms arise in all equations for which the test function is nonzero along a portion of the spatial boundary. As illustrated in the development for arbitrary Courant number presented in the appendix, equations associated with all nodes to the left of node $Nc + 2$ will have contributions from the inflow boundary (assuming constant Δx and V), where Nc is the (truncated) integer value of the Courant number Cu. For the present case of $1 \le \mathrm{Cu} < 2$, $Nc = 1$ and equations associated with w_0^{n-1}, w_1^{n+1}, and w_2^{n+1} will have boundary contributions. The relevant ELLAM equations for w_0^{n+1} and w_2^{n+1} are, respectively,

$$\int_{x_0}^{x_1} u(x, t^{n+1}) w_0^{n+1}(x, t^{n+1})\, dx - V \int_{t_1^*}^{t^{n-1}} u(0, t) w_0^{n+1}(0, t)\, dt - D\left[\left(\frac{-1}{\Delta x}\right) \int_{t_1^*}^{t^{n-1}} u(0, t)\, dt + \left(\frac{1}{\Delta x}\right) \int_{t_1^*}^{t^{n-1}} u(x_r^0(t), t)\, dt \right] + D \int_{t_1^*}^{t^{n-1}} \frac{\partial u}{\partial x}(0, t) w_0^{n+1}(0, t)\, dt = \int_{\Omega_2^0} f w_0^{n+1}\, dx\, dt \quad (15a)$$

and,

$$\int_{x_1}^{x_2} u(x, t^{n+1}) w_2^{n+1}(x, t^{n+1})\, dx - \left[\int_{x_0}^{x_1^*} u(x, t^n) w_2^{n-1}(x, t^n)\, dx + V \int_{t^n}^{t_1^*} u(0, t) w_2^{n+1}(0, t)\, dt \right] - D\left[\left(\frac{1}{\Delta x}\right) \int_{t_1^*}^{t^{n-1}} u(x_l^2(t), t)\, dt - \left(\frac{2}{\Delta x}\right) \int_{t^n}^{t^{n-1}} u(x_c^2(t), t)\, dt + \left(\frac{1}{\Delta x}\right) \int_{t^n}^{t^{n-1}} u(x_r^2(t), t)\, dt \right] + D \int_{t^n}^{t_1^*} \frac{\partial u}{\partial x}(0, t) w_2^{n+1}(0, t)\, dt - D\left(\frac{1}{\Delta x}\right) \int_{t^n}^{t_1^*} u(0, t)\, dt = \int_{\Omega_1^1 \cup \Omega_2^1} f w_2^{n+1}\, dx\, dt. \quad (15b)$$

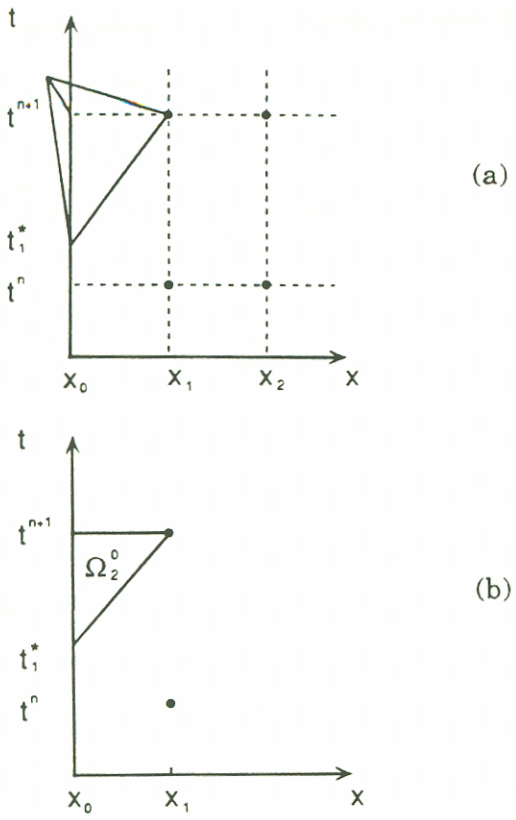

Fig. 3. (a) Test function $w_0^{n+1}(x, t)$, and (b) associated geometric definitions

Equations (14), (15a), and (15b) are the three equations (for $Nc = 1$) in which inflow boundary conditions appear. If a first-type boundary condition is specified, then all integrals involving $u(0, t)$ are known and the integrals involving the diffusive flux $D(\partial u/\partial x)(0, t)$ are unknown. Conversely, for a second-type boundary condition, $(\partial u/\partial x)(0,t)$ is known and $u(0, t)$ must be determined. Finally, for a third-type boundary conditions, the gradient $(\partial u/\partial x)(0, t)$ may be written in terms of $u(0, t)$, or vice versa. For all three scenarios, both u and $(\partial u/\partial x)$ must be determined at the inflow boundary, and equation (15a) is therefore required. Notice that in all three equations ((14), (15a), (15b)) the advective and diffusive fluxes may be combined: in equation (15a), for example, the total boundary flux term is

$$-\int_{t_1^*}^{t^{n+1}} \left[Vu(0, t) - D \frac{\partial u}{\partial x}(0, t) \right] w_0^{n+1}(0, t)\mathrm{d}t.$$

This is convenient for implementation of third-type boundary conditions and also makes it easier to see that the final set of equations possesses the conservative property (see Section 5). In addition, if a one-point integration rule is used to approximate the boundary integrals, and the integration point is $t = t^{n+1}$, then the flux term in, for example, equation (14),

$$\int_{t^n}^{t^{n+1}} \frac{\partial u}{\partial x}(0, t) w_1^{n+1}(0, t)\mathrm{d}t,$$

is zero because $w_i^{n+1}(0, t^{n+1}) = 0$ for all $i > 0$. Therefore, while this diffusive type of boundary integral is present in all ELLAM equations that have characteristics that intersect the inflow boundary, further approximation of the equations may eliminate this term. This point appears to have significance for the resulting matrix structure, as discussed in Section 5.

Notice that, in general, when a characteristic crosses the boundary, some of the integrals that arise in the ELLAM equations span a time less than Δt. In particular, the integrals related to the diffusion term (for example, the third and fourth integrals in equation (15a)) span the time increment $t^{n+1} - t_1^*$, which is less than Δt. Thus the diffusion part of the equation applies over a reduced time step. This effect, which was unnoticed by most CM references in the literature (an exception being Douglas *et al.*[20]), arises naturally in the ELLAM formulation.

These issues about the one-point integration and time intervals less than Δt are discussed further, from a different point of view, by Russell[43]. There, an equivalent formulation is derived, in which the terms multiplied by D in equations (14), (15a), and (15b) are obtained by integrating the diffusive term in equation (8) by parts once instead of twice. Russell's paper emphasizes the special case of ELLAM with one-point integration as an extension of MMOC.

Treatment of outflow boundary conditions is somewhat more involved. We herein propose an approach that inherently conserves global mass and directly accommodates the case of pure advection (D = 0), for which no outflow boundary condition is specified. To begin, let

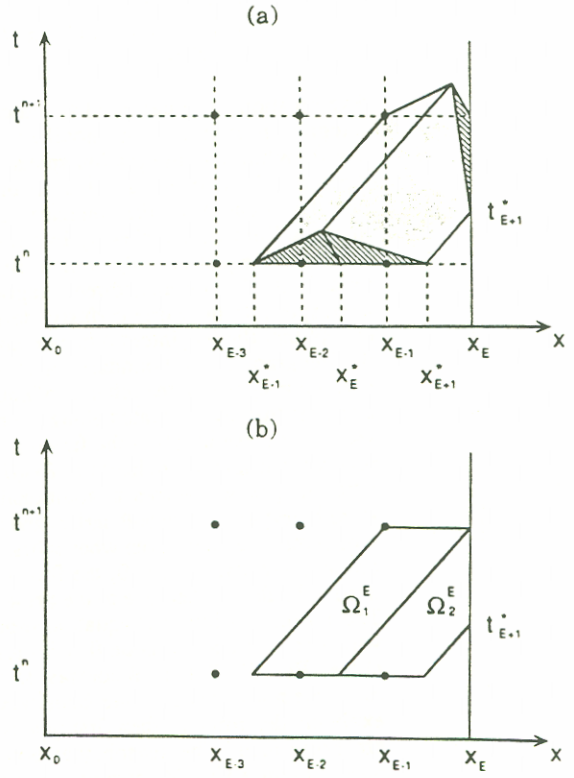

Fig. 4. (a) Test function $w_E^{n+1}(x, t)$, and (b) associated geometric definitions

the boundary condition of equation (3), namely $(\partial u/\partial x)(l, t) = q_l(t)$, pertain. Again, consider the case of $1 \le Cu < 2$, so that $Nc = 1$. ELLAM equations would be written for nodes $x_0, x_1, x_2, \ldots, x_{E-1}$; equations (14), (15a), and (15b) provide expressions for $i = 0, 1, 2$, respectively, while equation (9) applies for $i = 3, 4, \ldots, E-1$. If the only unknowns in these equations are nodal values at the new time level, then these equations constitute a set of E equations in $E+2$ unknowns (unknowns $(\partial U_0^{n+1}/\partial x)$, U_0^{n+1}, U_1^{n+1}, U_2^{n+1}, $\ldots$, U_E^{n+1}). One additional equation is available from the inflow boundary condition. If a first-type boundary condition were given at $x = l$, then U_E^{n+1} would also be known and, coupled with the boundary condition at $x = 0$, the system could be solved for all nodal unknowns listed above. However, if a second-type boundary condition is prescribed, then U_E^{n+1} is not known and an additional equation must be written, that associated with $w_E^{n+1}(x, t)$. The function $w_E^{n+1}(x, t)$ is illustrated in Fig 4. Notice that this is the first test function that has a nonzero region along $x = x_E = l$, $t^n \le t \le t^{n+1}$. Therefore boundary terms at $x = l$ will appear in this equation. Evaluation of the ELLAM equation for w_E^{n+1} leads to the following expression:

$$\int_{x_{E-1}}^{x_L} u(x, t^{n+1}) w_E^{n+1}(x, t^{n+1})\, dx + V\int_{t_{E-1}^*}^{t^{n+1}} u(l, t) w_E^{n+1}(l, t)\, dt \Big] - \int_{x_{E-1}^*}^{x_L} u(x, t^n) w_E^{n+1}(x, t^n)\, dx - D\Big[\Big(\frac{1}{\Delta x}\Big)\int_{t^n}^{t^{n+1}} u(x_l^E(t), t)\, dt - \Big(\frac{2}{\Delta x}\Big)\int_{t^n}^{t^{n+1}} u(x_c^E(t), t)\, dt + \Big(\frac{1}{\Delta x}\Big)\int_{t^n}^{t_{E-1}^*} u(x_r^E(t), t)\, dt\Big] - D\int_{t_{E-1}^*}^{t^{n+1}} \frac{\partial u}{\partial x}(l, t) w_E^{n+1}(l, t)\, dt - D\Big(\frac{1}{\Delta x}\Big)\int_{t_{E-1}^*}^{t^{n+1}} u(l, t)\, dt = \int_{\Omega_1^E \cup \Omega_2^E} f w_E^{n+1}\, dx\, dt. \quad (16)$$

For a second-type boundary condition, $(\partial u/\partial x)(l, t)$ would be prescribed as the outflow boundary condition while $u(l, t)$ is unknown for $t^n < t \le t^{n+1}$. One possibility for evaluation of $u(l, t)$, $t^n < t \le t^{n+1}$, is a simple interpolation between U_E^n and U_E^{n+1}. Then, no additional unknown is introduced in equation (16), and the system of equations would be closed. Another option is to place an additional node at the location (x_E, t_{E-1}^*), and to define an additional nodal unknown at this point. For the latter case, let a node be added at location (x_E, t_{E-1}^*), call it node α_1, with the associated discrete unknown denoted by U_{α_1}. Because this adds another unknown to the system, another algebraic equation must be sought. To achieve this, an ELLAM equation can be written for the test function $w_{E-1}^{n+1}(x, t)$, with only that portion of the test function within the domain Ω_{α_1} used for the approximation (see Fig. 5). Use of $w_{E-1}^{n+1}(x, t)$ as the test function leads to the following ELLAM equation:

$$V\int_{t^n}^{t^{n+1}} u(l, t) w_{E-1}^{n+1}(l, t)\, dt - \int_{x_E^*}^{x_L} u(x, t^n) w_{E-1}^{n+1}(x, t^n)\, dx - D\Big[\Big(\frac{1}{\Delta x}\Big)\int_{t^n}^{t^{n+1}} u(x_l^{E-1}(t), t)\, dt - \Big(\frac{2}{\Delta x}\Big)\int_{t^n}^{t_{E-1}^*} u(x_c^{E-1}(t), t)\, dt\Big] - D\int_{t^n}^{t^{n+1}} \frac{\partial u}{\partial x}(l, t) w_{E-1}^{n+1}(l, t)\, dt + D\Big(\frac{1}{\Delta x}\Big)\Big[\int_{t_{E-1}^*}^{t^{n+1}} u(l, t)\, dt - \int_{t^n}^{t_{E-1}^*} u(l, t)\, dt\Big] = \int_{\Omega_1^{E-1} \cup \Omega_2^{E-1}} f w_{E-1}^{n+1}\, dx\, dt. \quad (17)$$

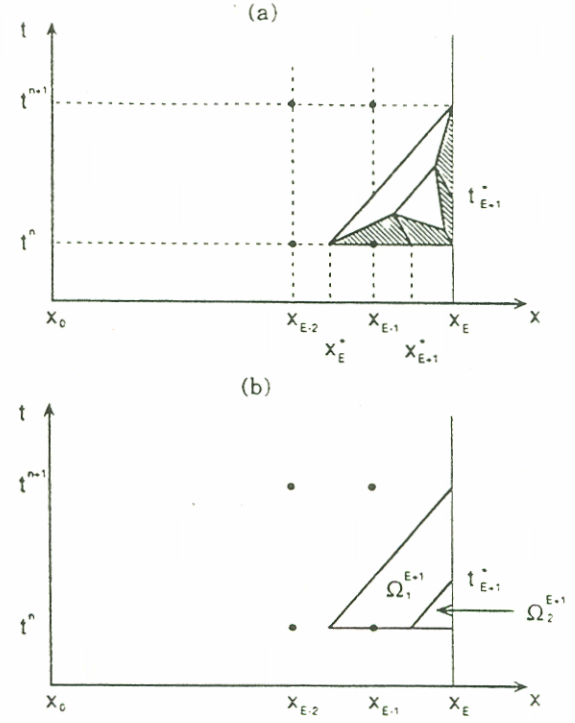

Fig. 5. (a) Test function $w_{E-1}^{n+1}(x, t)$, and (b) associated geometric definitions

Integrals along the boundary $x = x_E = l$ can again be approximated using discrete nodal values. Because $w_{E+1}^{n+1}(l, t)$ is nonzero at $t = t^n$, and all information is assumed known for $t \le t^n$, it is this information at node E and time t^n that effectively serves to close the system. For this case of second-type outflow boundary conditions and $Nc = 1$, there are $E + 2$ ELLAM equations written, corresponding to w_0^{n+1}, w_1^{n+1}, . . . , w_{E+1}^{n+1}. These are solved for the nodal unknowns $(\partial U_0^{n+1}/\partial x)$, U_i^{n+1}, U_2^{n+1}, . . . , U_E^{n+1}, U_{α_l}. The nodal values that are known are U_0^{n+1} (from the inflow boundary condition); $(\partial U_E^{n+1}/\partial x)$, $(\partial U_{\alpha_l}/\partial x)$, and $(\partial U_E^n/\partial x)$ (from the outflow boundary condition); and U_E^n (from the solution at the previous time step).

While these equations provide a solution for the unknowns of interest, they generally fail to conserve global mass. The next section addresses the question of mass conservation and presents a modification to these equations so that the resulting set of ELLAM equations possesses the conservative property.

5. GLOBAL MASS CONSERVATION

This section examines the global mass conservation properties of the ELLAM algorithm. As was done in the previous sections, the case of $Nc = 1$ will be used as an example. The general case is presented in the appendix.

To analyze mass balance, consider summation of all ELLAM equations. Summation of equations associated with test functions w_0^{n+1} through w_{E+1}^{n+1} results in the following expression.

$$\begin{aligned}
&\int_{x_0}^{x_E} u(x, t^{n+1})\, dx - \left[\int_{x_0}^{x_{E-1}^*} u(x, t^n)\, dx \right. \\
&\quad \left. + \int_{x_{E-1}^*}^{x_E} u(x, t^n) w_{E+1}^{n+1}(x, t^n)\, dx \right] \\
&\quad - \int_{t^n}^{t^{n+1}} \left[Vu(0, t) - D \frac{\partial u}{\partial x}(0, t) \right] dt \\
&\quad + \int_{t_{E-1}^*}^{t^{n+1}} \left[Vu(l, t) - D \frac{\partial u}{\partial x}(l, t) \right] dt \\
&\quad + \int_{t^n}^{t_{E-1}^*} \left[Vu(l, t) \right. \\
&\quad \left. - D \frac{\partial u}{\partial x}(l, t) \right] w_{E+1}^{n+1}(x, t)\, dt \\
&\quad - D\left(\frac{1}{\Delta x}\right) \int_{t^n}^{t_{E-1}^*} u(l, t)\, dt \\
&\quad + D\left(\frac{1}{\Delta x}\right) \int_{t^n}^{t_{E-1}^*} u(x_c^{E+1}(t), t)\, dt \\
&= \int_{t^n}^{t^{n+1}} \int_{x_0}^{x_E} f(x, t)\, dx\, dt \\
&\quad - \int_{\Omega_2^{E+1}} f(x, t)[1 - w_{E+1}^{n+1}(x, t)]\, dx\, dt. \qquad (18)
\end{aligned}$$

In equation (18), use was made of the fact that within any space-time element $\Omega_1^k = \Omega_2^{k-1}$ and $w_k^{n+1} + w_{k-1}^{n+1} = 1$. In addition, $\Sigma_{i=0}^{E} w_i^{n+1}(x, t^{n+1}) = 1$ $(0 \le x \le l)$ and $\Sigma_{i=0}^{E} w_i^{n+1}(0, t) = 1$ $(t^n \le t \le t^{n+1})$. Examination of equation (18) indicates that a global balance is almost achieved, with boundary and interior regions associated with space-time element Ω_2^{E+1} being responsible for the lack of global balance. This can be explained as follows. Within any space-time element that is bounded by nodes x_k and x_{k-1} at time t^{n+1}, two test functions will be nonzero, namely w_k^{n+1} and w_{k-1}^{n+1}. Because these functions sum to one within the element, and because of the symmetries in the boundary integral terms, the sum of the two ELLAM equations associated with these two test functions preserves a global balance. Element Ω_2^{E+1} suffers from the lack of an ELLAM equation associated with test function $w_{E+2}^{n+1}(x, t)$. In fact, w_{E+2}^{n+1} is the only remaining test function that has a nonzero region in $[0, l] \times [t^n, t^{n+1}]$ for which an ELLAM equation has not been written. The ELLAM equation associated with w_{E+2}^{n+1} is not needed to solve for the nodal unknowns of interest, because the known values from the previous time level at node E in effect supersede this equation. However, this final equation can be used to enforce global mass conservation.

The test function $w_{E+2}^{n+1}(x, t)$ is illustrated in Fig. 6. The ELLAM equation associated with test function $w_{E+2}^{n+1}(x, t)$ is

$$\begin{aligned}
&\int_{t^n}^{t_{E-1}^*} \left[Vu(l, t) - D \frac{\partial u}{\partial x}(l, t) \right] w_{E+2}^{n+1}(l, t)\, dt \\
&\quad - \int_{x_{E-1}^*}^{x_E} u(x, t^n) w_{E+2}^{n+1}(x, t^n)\, dx \\
&\quad + D\left(\frac{1}{\Delta x}\right) \left[\int_{t^n}^{t_{E-1}^*} u(l, t)\, dt \right. \\
&\quad \left. - \int_{t^n}^{t_{E-1}^*} u(x_l^{E+2}(t), t)\, dt \right] \\
&= \int_{\Omega_1^{E+2}} f(x, t) w_{E+2}^{n+1}(x, t)\, dx\, dt. \qquad (19)
\end{aligned}$$

Summation of equations (18) and (18) yields

$$\begin{aligned}
&\int_{x_0}^{x_E} u(x, t^{n+1})\, dx - \int_{x_0}^{x_E} u(x, t^n)\, dx \\
&\quad - \int_{t^n}^{t^{n+1}} \left[Vu(0, t) - D \frac{\partial u}{\partial x}(0, t) \right] dt \\
&\quad + \int_{t^n}^{t^{n+1}} \left[Vu(l, t) - D \frac{\partial u}{\partial x}(l, t) \right] dt \\
&= \int_{t^n}^{t^{n+1}} \int_{x}^{x_E} f(x, t)\, dx\, dt, \qquad (20)
\end{aligned}$$

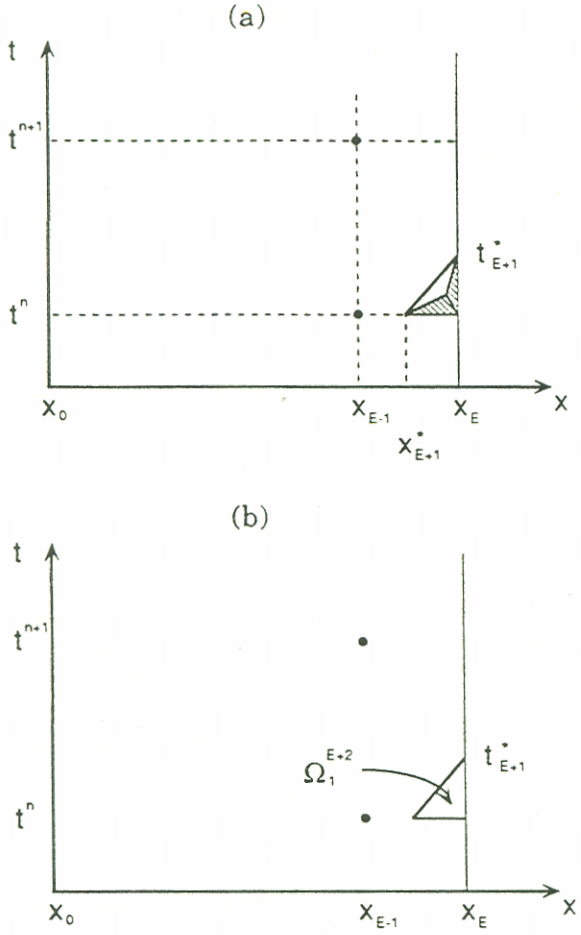

Fig. 6. (a) Test function $w_{E-2}^{n-1}(x, t)$, and (b) associated geometric definitions

which represents a statement of global mass conservation. Therefore, the set of all ELLAM equations, including that associated with $w_{E-2}^{n-1}(x, t)$, possesses the conservative property. However, use of all ELLAM equations overspecifies the system by one equation. Yet without equation (19), the ELLAM system does not, in general, possess the conservative property. Therefore, add equation (19) to equation (17), noting that $x_l^{E+2}(t) = x_c^{E+1}(t)$, $\Omega_1^{E+2} = \Omega_2^{E+1}$, and $w_{E-1}^{n+1}(x, t) + w_{E+2}^{n+1}(x, t) = 1$ on Ω_2^{E+1} (see Figs 5 and 6). This yields

$$\left[\int_{t_{L-1}^*}^{t^{n+1}} \left[Vu(l, t) - D\frac{\partial u}{\partial x}(l, t)\right] w_{E-1}^{n+1}(l, t)\, dt + \int_{t^n}^{t_{L-1}^*} \left[Vu(l, t) - D\frac{\partial u}{\partial x}(l, t)\right] dt\right] - \left[\int_{x_L^*}^{x_{L-1}^*} u(x, t^n) w_{E-1}^{n+1}(x, t^n)\, dx + \int_{x_{L-1}^*}^{x_L} u(x, t^n)\, dx\right] + D\left(\frac{1}{\Delta x}\right)\int_{t_{L-1}^*}^{t^{n+1}} u(l, t)\, dt - D\left[\left(\frac{1}{\Delta x}\right)\int_{t^n}^{t^{n+1}} u(w_l^{E-1}(t), t)\, dt - \left(\frac{1}{\Delta x}\right)\int_{t^n}^{t_{L-1}^*} u(x_c^{E-1}(t), t)\, dt\right] = \int_{\Omega_2^{E-1}} f w_{E-1}^{n+1}\, dx\, dt + \int_{\Omega_2^{E-1}} f(x, t)\, dx\, dt. \quad (21)$$

If equation (21) is used in place of equation (17), then the proper number of ELLAM equations results and these equations possess the conservative property by summing to equation (20) instead of equation (19).

The modifications presented above guarantee mass conservation for the system of equations that includes U_{α_1} as an unknown. Recall that this was one of two options presented in Section 4, the other being simple interpolation between t^n and t^{n+1} along the outflow boundary. If this other option is chosen, global mass conservation can still be achieved. This is accomplished by using the information contained in the ELLAM equations associated with w_{E-1}^{n+1} and w_{E-2}^{n+1}. In this case, these two equations (equations (17) and (19)) should be summed and then added to the equation associated with w_E^{n+1} (equation (16)) to obtain

$$\int_{x_{L-1}}^{x_L} u(x, t^{n+1}) w_E^{n+1}(x, t^{n+1})\, dx + \int_{t^n}^{t^{n+1}} \left[Vu(l, t) - D\frac{\partial u}{\partial x}(l, t)\right] dt - \left[\int_{x_L^*}^{x_{L-1}^*} u(x, t^n) w_E^{n+1}(x, t^n)\, dx + \int_{x_{L-1}^*}^{x_L} u(x, t^n)\, dx\right] - D\left[\left(\frac{1}{\Delta x}\right)\int_{t^n}^{t^{n+1}} u(x_l^E(t), t)\, dt - \left(\frac{1}{\Delta x}\right)\int_{t^n}^{t^{n+1}} u(x_c^E(t), t)\, dt\right] = \int_{\Omega_1^{n+1}} f w_E^{n+1}\, dx\, dt + \int_{\Omega_1^{n+1} \cup \Omega_2^{n+1}} f\, dx\, dt. \quad (22)$$

Just as equation (19) modified equation (17) to provide a conservative scheme when U_{α_1} was included, now the sum of equations (17) and (19) injects information into equation (16) so that global mass conservation is guaranteed.

In general, ELLAM equations should be written for all test functions that have nonzero values within $[x_0, x_E] \times [t^n, t^{n+1}]$. For the case of $Nc = 1$, this means w_0^{n+1}

through w_{E+2}^{n+1}. If a first-type boundary condition is given at the outflow boundary, then the first E equations may be solved independently. If detailed information about $(\partial u/\partial x)$ at the outflow boundary is desired, then the additional equations should be written and solved for nodal values of $(\partial U_E^{n+1}/\partial x)$ and $(\partial U_{\alpha_1}/\partial x)$, subject to the global conservation constraint imposed by the equation associated with w_{E+2}^{n+1}. If only a measure of the total flux crossing the boundary is of interest, the additional equations may be summed to give a relationship between total outflux and known information. For the case of $Nc = 1$, rearrangement of equation (22) yields

$$\begin{aligned}\int_{t^n}^{t^{n+1}} \left[Vu(l, t) - D \frac{\partial u}{\partial x}(l, t) \right] dt &= \int_{\Omega_1^E} f w_E^{n+1}\, dx\, dt \\ &+ \int_{\Omega_1^{E-1} \cup \Omega_1^{E-2}} f(x, t)\, dx\, dt \\ &+ D\left[\left(\frac{1}{\Delta x}\right) \int_{t^n}^{t^{n+1}} u(x_I^E(t), t)\, dt \right. \\ &\left. - \left(\frac{1}{\Delta x}\right) \int_{t^n}^{t^{n+1}} u(x_c^E(t), t)\, dt \right] \\ &+ \int_{x_{E-1}^*}^{x_E^*} u(x, t^n) w_E^{n+1}(x, t^n)\, dx \\ &+ \int_{x_E^*}^{x_E} u(x, t^n)\, dx \\ &- \int_{x_{I-1}}^{x_I} u(x, t^{n+1}) w_E^{n+1}(x, t^{n+1})\, dx. \end{aligned} \tag{23}$$

All information on the right side of equation (23) is known from the previous solution of the first E ELLAM equations, so that the total flux may be calculated.

For a second- or third-type boundary condition at the outflow boundary, the equation associated with w_E^{n+1} must be written. Evaluation of the boundary flux terms may then proceed by introduction of the additional unknown U_{α_1}, as illustrated in Section 4, or by interpolation between time levels n and $n + 1$. If the latter case is chosen, then equation (16) would be replaced by equation (22). Otherwise, equation (19) is summed with equation (17) as demonstrated in equation (21). In all of these cases, global mass conservation is assured.

Notice that summation of equations produces a result that is equivalent to deriving the ELLAM equations using a redefined test function. This redefined test function is equal to the sum of the original test functions. For example, combination of equations (17) and (19) results in equation (21); equation (21) can also be obtained by application of ELLAM using the modified test function $w^* \equiv w_{E+1}^{n+1} + w_{E+2}^{n+1}$, which has the definition,

$$w^*(x, t) = \begin{cases} \dfrac{x - x_E}{\Delta x} + \dfrac{t^{n+1} - t}{\Delta x}, & (x, t) \in \Omega_1^{E+1}, \\ 1, & (x, t) \in \Omega_2^{E+1}, \\ 0, & \text{all other } (x, t). \end{cases}$$

Similarly, the combination of equations (16), (17), and (19) (which eliminates U_{α_1}) can be achieved using ELLAM with test function $w^{**} \equiv w_E^{n+1} + w_{E+1}^{n+1} + w_{E+2}^{n+1}$,

$$w^{**}(x, t) = \begin{cases} \dfrac{x - x_{E-1}}{\Delta x} + \dfrac{t^{n+1} - t}{\Delta x}, & (x, t) \in \Omega_1^E, \\ 1, & (x, t) \in \Omega_2^E \text{ or } (x, t) \in \Omega_2^{E+1}, \\ 0, & \text{all other } (x, t). \end{cases}$$

The redefined test functions still satisfy the homogeneous adjoint equation within each element.

While the ELLAM procedure provides a variety of choices for dealing with boundary conditions, the procedure can always incorporate all types of possible boundary conditions and guarantee that a conservative scheme will result. In general, when a first-type boundary condition is given at the inflow boundary, equations associated with w_0^{n+1} and w_i^{n+1} $(1 \le i < E)$ should be written. The first $Nc + 2$ of these equations will include boundary values of both u and $(\partial u/\partial x)$. When a one-point fully implicit approximation is used for these boundary integrals, the flux integral only appears in the first (w_0^{n+1}) equation, so that it is not necessary to solve for the unknown $(\partial u/\partial x)$ at t^{n+1}. The ELLAM equation associated with w_0^{n+1} is uncoupled from the others in this case, and only needs to be used to calculate the inflow boundary flux, if desired. As in the outflow case just described, this may be done by replacing w_1^{n+1} with the sum $w_0^{n+1} + w_1^{n+1}$, which is equal to one on Ω_1^1. When a second- or third-type boundary condition is specified at the inflow boundary, the equation associated with w_0^{n+1} must be used, independent of the boundary integration method chosen. The outflow boundary is similar to the inflow boundary in that no boundary equations are required when a first-type condition is specified. Boundary equations, associated with w_E^{n+1}, w_{E+1}^{n+1}, . . . , are required only to calculate the associated outflow boundary flux. For flux boundary conditions, at least one outflow boundary equation must be written, that being the equation based on the summed test functions. If more refined information is desired at the outflow boundary, individual equations may be written for w_E^{n+1}, w_{E+1}^{n+1}, . . . , with concomitant introduction of additional unknowns analogous to U_{α_1} above. These procedures yield Eulerian-Lagrangian schemes that demonstrably possess the conservative property.

A final consideration in boundary condition implementation is the matrix structure of the resulting set of algebraic equations. This depends on the choice of trial function, call it $\hat{u}$, that is used to approximate the unknown function u. So far, the trial function has not been specified, except in the MMOC example of equation (13). In view of the test functions, which have the chapeau form at $t = t^{n+1}$, it is natural to define $\hat{u}$ to be piecewise linear also. Interpolation between $t = t^n$ and $t = t^{n+1}$ can be taken to be linear along characteristic lines. For one-space-dimensional problems, this gives rise to the general matrix structure illustrated in Fig. 7. The matrix is symmetric, tridiagonal except for the additional column of potentially nonzero entries associated with inflow boundary information. This corresponds to the unknown at the inflow

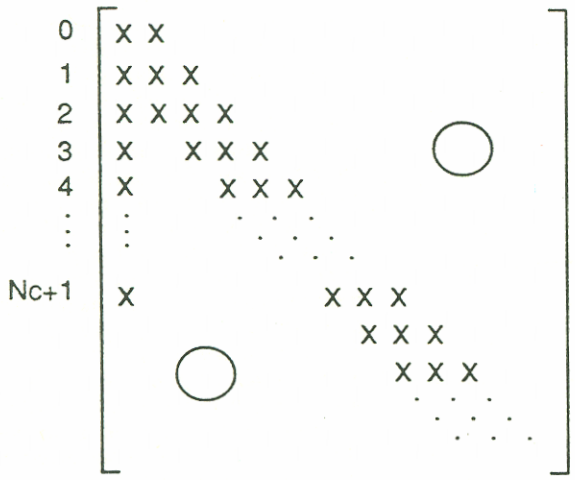

Fig. 7. General matrix structure for ELLAM. Nc is the truncated integer value of the Courant number

boundary: $(\partial U_0^{n-1}/\partial x)$ for Dirichlet problems and U_0^{n+1} for Neumann or Robin problems. This column (except for the entry in row one) may be eliminated in the Dirichlet problem via judicious one-point approximations to the integrals involving $(\partial u/\partial x)(0, t)$. Elimination of this column is more difficult in the other cases of second- or third-type boundary conditions because it appears that larger errors are committed in achieving this, although quantitative demonstration of this point remains to be done.

Notice that the matrix structure depends entirely on the chosen interpolation (integration) rule, which is dictated by choice of trial function. For example, a space-time interpolation that does not follow characteristic lines will in general lead to less sparseness in the matrix stucture, accompanied by loss of symmetry. This is an important consideration because the computational advantages in maintaining a symmetric tridiagonal matrix are significant, while the accuracy of the method depends heavily on the chosen interpolation. Further analysis is required to adequately resolve this issue.

6. THE CASE OF PURE ADVECTION

The ELLAM equations presented in Sections 3 through 5 naturally accommodate the degenerate case of $D = 0$. The approach incorporates all of the space-time domain of interest and uses known information from the previous time step (U_E^n) to close the system of discrete equations. The ELLAM equations remain exactly as written in Sections 3, 4, and 5, with any terms multiplied by D simply set to zero. All terms involving spatial gradients $(\partial u/\partial x)$ disappear because they are all multiplied by D (actually these terms never arise because the second-order diffusive term is absent in the governing equation). Unknowns are now $\{U_1^{n+1}, U_2^{n+1}, \ldots, U_E^{n+1}, U_{a_i}\}$ (assuming $Nc = 1$). A first-type boundary condition is required at $x = 0$, since the governing equation is now formally first-order. Therefore U_0^{n-1} will be known. Notice that the test functions continue to satisfy the homogeneous adjoint equation within each space-time element. This is why the ELLAM equations can be used directly as written above. The ELLAM equations therefore inherently accommodate a formal change of governing from a second-order parabolic equation in which boundary conditions are specified at both inflow and outflow boundaries to a first-order hyperbolic equation in which boundary conditions are given only at inflow boundaries. No change is required in the ELLAM algorithm.

7. EXAMPLE CALCULATIONS

This section reports on computations with ELLAM for a simple test problem. As noted in Section 3, a backward Euler approximation of the temporal integrals in interior elements yields the MMOC procedure, given by equation (13). The benefit of ELLAM in this context is that it shows how to treat boundary conditions (Section 4) and conserve mass (Section 5). Numerical results applying MMOC to equation (3) have appeared previously[22], but that work did not address boundary conditions, since the computational boundaries were far from the advecting front. Hence, mass conservation, which did hold in the earlier work, was not studied in a situation where boundaries were important.

With this background, the natural experiments to perform here are ones that include significant boundary behaviour. We consider an advecting Gaussian hill that may cross an inflow or outflow boundary. Specifically, we solve equation (3) with $f = 0$ and initial condition

$$u_I(x) = \exp(-\pi x^2) \tag{24}$$

chosen so that the initial peak value of u and total mass are both equal to 1. As a pure initial-value problem, this leads to the analytical solution

$$u_a(x, t) = \frac{1}{\sqrt{1 + 4\pi Dt}} \exp\left(\frac{-\pi(x - Vt)^2}{1 + 4\pi Dt}\right). \tag{25}$$

We obtain an initial-boundary-value problem with the same solution by cutting off the spatial domain and imposing Dirichlet or flux boundary conditions from equation (25), viz.,

$$u(a, t) = u_a(a, t)$$

or

$$\left(Vu - D\frac{\partial u}{\partial x}\right)(a, t) = \left(Vu_a - D\frac{\partial u_a}{\partial x}\right)(a, t), \tag{26}$$

$$u(b, t) = u_b(b, t),$$

or

$$\left(Vu - D\frac{\partial u}{\partial x}\right)(b, t) = \left(Vu_a - D\frac{\partial u_a}{\partial x}\right)(b, t), \tag{27}$$

where $\Omega_x = [a, b]$ is the truncated spatial domain.

In the runs to be reported here, we used $V = 10$, $D = 0.1$, and final time $t_f = 0.5$. Thus, the peak traveled from $x = 0$ to $x = 5$, over which distance the Peclet number was 500. Some runs with $D = 0.001$, or Peclet number 50,000, were also made. The exact solutions in these cases are shown in Fig. 8. We considered the

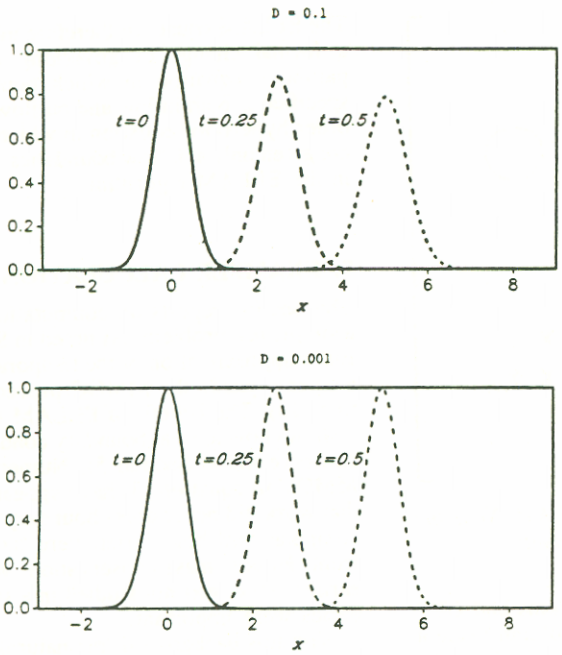

Fig. 8. Exact solution for example problem (equation (25)) with (a) D = 0.1, and (b) D = 0.001

domains $[2\frac{1}{3}, 9]$, $[-3, 2\frac{1}{3}]$, and $[-3, 9]$, with which, respectively, the pulse crosses an inflow boundary, an outflow boundary, or neither; denote the domains by *I*, *O*, and *N*. For each domain, all relevant combinations of boundary conditions were tried. The maximum slope of the initial pulse is $\sqrt{2\pi/e} \approx 1.52$, and at $t = t_f$ it is $\sqrt{(2\pi/e)}/(1 + 4\pi D t_f) \approx 0.933$ ($D = 0.1$) or 1.51 ($D = 0.001$) with peak value $1/\sqrt{1 + 4\pi D t} \approx 0.784$ ($D = 0.1$) or 0.997 ($D = 0.001$).

Previous numerical studies of MMOC with linear trial functions have demonstrated that it produces accurate, nonoscillatory results as long as at least three intervals discretize a front. In the context of a Gauss hill of peak value 1, we take this to mean that Δx should be no larger than $1/3S$, were S is the maximum slope; in our case this is $\sqrt{e}/18\pi \approx 0.219$. Our runs showed that we could do slightly better than this, and $\Delta x = 4/15 \approx 0.267$ was used as a base case. This corresponds to a grid Peclet number $Pe = V\Delta x/D = 26\frac{2}{3}$. As a check on convergence rates, we also ran with the 5-fold refinement $\Delta x = 4/75 \approx 0.0533$ [$Pe = 5\frac{1}{3}$]. For $\Delta x = 4/15$, we used $\Delta t = 0.25$ and 0.05 (Cu = $9\frac{3}{8}$, $1\frac{7}{8}$); for $\Delta x = 4/75$, $\Delta t = 0.25$, 0.05, 0.01, and 0.002 (Cu = $46\frac{7}{8}$, $9\frac{3}{8}$, $1\frac{1}{7}$, $\frac{3}{8}$) were run.

In order to assess the effectiveness of ELLAM in the absence of quadrature errors, we computed integrals involving initial and boundary conditions with high-order Lobatto rules. For example, in equation (14), the second integral involves initial conditions when $n = 0$, and the third and seventh integrals combine into a flux boundary condition (for a Dirichlet condition, the third integral uses the boundary data, while the seventh becomes a spatial integral at time level $n + 1$ under a backward Euler scheme detailed in Ref. 43). Similarly, in equation (17), the first, second, and fifth integrals are of these types, and the second integral in equation (9) uses $u_f(x)$ when $n = 0$. For $n > 0$, as noted in Section 3, the integrals at $t = t^n$ can be evaluated exactly, and this was done here. Integrals such as the first in equation (9) were computed exactly, and temporal integrals were replaced by backward Euler approximations in order to obtain the MMOC procedure. With these specifications, all calculations conserved mass to the level of machine roundoff.

In the computations, we found it advantageous to consolidate the last two outflow-boundary elements described in Section 4 into a single element. That is, instead of Nc trapezoids and one small triangle along the outflow boundary, we have $Nc - 1$ trapezoids and one larger triangle. This corresponds to use of the function w^{**} in Section 5, and avoids the possibility of anomalous answers on the small triangle. For a Dirichlet outflow condition, as noted in Section 5, ELLAM solves for the outgoing flux as a function of time; we considered piecewise-linear and piecewise-constant representations of this function. For full details of the implementation, see Ref. 43.

Results for the test runs are summarized in Table 1. All runs used $D = 0.1$ except for those designed by '*d*', which took $D = 0.001$. For the domains *N* and *I*, L^2 errors and peak values are given at the final time $t_f = 0.5$. For O, these are listed at $t = 0.25$, at which time the peak is leaving the domain. This time usually provided the least favorable (i.e., largest) ratio of the L^2 error of the numerical solution to that of the L^2 projection; this ratio is necessarily at least 1. In runs 25 through 30, the peak has left and the Dirichlet outflow condition forces the numerical maximum to agree with the exact one, rendering peak-value data meaningless.

Runs 1 through 6 do not involve significant boundary behaviour, so that the implemented ELLAM reduces to MMOC and we find results analogous to those reported by Ewing and Russell[22]. Comparing runs 5 and 6, we see that temporal error is relatively unimportant, so that we can conclude $0(\Delta x^2)$ convergence by relating run 1 to 5 or 2 to 6. Similarly, spatial error is unimportant in runs 3 and 4 and we find a rate of $0(\Delta t)$. Runs 1 and 2, with a spatial mesh of the size that one would want in practice, show that large Courant numbers are appropriate with this scheme. The peak in excess of 1 in run 2*d* is not an instability; as the L^2 projection shows, it is a necessary result of accurate approximation of a peak by continuous piecewise-linear polynomials on a course grid. By examining the difference between the numerical peak value and the L^2-projection peak for fixed Δx and variable Δt, we see that time truncation is antidiffusive; with variable Δx and fixed Δt, spatial error is found to be diffusive.

Runs 7 through 18, with domain I, demonstrate that we can move the peak through the inflow boundary about as well as possible. Comparison of runs 7 through 12, as a group, to 13 through 18 shows that the type of boundary condition makes virtually no difference. The L^2 error tends to be slightly larger with a Dirichlet condition, especially in the lower-diffusion run 8*d*. This is easily explained by noting that the essential condition is imposed exactly at the boundary node, while better L^2 accuracy during the passage of the peak could be obtained if the boundary value were free as in the flux-condition case. For related reasons, runs 8 and 8d show miniscule oscillations (of size about 0.0001 and 0.001, respectively) ahead of the peak as it enters; diffusion subsequently eliminates